Journal of Power Sources 260 (2014) 205–210

Contents lists available at ScienceDirect

Journal of Power Sources

journal homepage: www.elsevier.com/locate/jpowsour

A facile synthesis of encapsulated $CoFe_2O_4$ into carbon nanofibres and its application as conversion anodes for lithium ion batteries

Shuhua Ren [a,*], Xiangyu Zhao [a,b], Ruiyong Chen [a], Maximilian Fichtner [a,c]

[a] Karlsruhe Institute of Technology (KIT), Institute of Nanotechnology (INT), Postbox 3640, 76021 Karlsruhe, Germany
[b] College of Materials Science and Engineering, Nanjing University of Technology, 210009 Nanjing, China
[c] Helmholtz Institute Ulm (HIU), Albert-Einstein Allee 11, 89081 Ulm, Germany

HIGHLIGHTS

- A solvent-free and template-free process yielded a fine $CoFe_2O_4$/C nanocomposite.
- The composite consists of in-situ formed carbon nanofibres encapsulated with cobalt ferrite nanoparticles.
- The carbon content can be easily adjusted by varying oxidation conditions.
- The conversion anode material gives more than 700 mAh g^{-1} after 250 cycles.
- Intimate connection between ferrite and carbon is crucial for the observing performance.

GRAPHICAL ABSTRACT

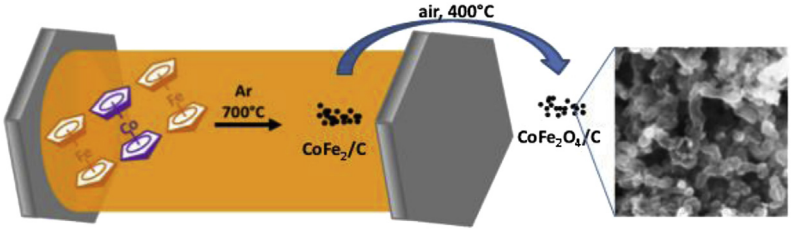

ARTICLE INFO

Article history:
Received 16 January 2014
Received in revised form
3 March 2014
Accepted 7 March 2014
Available online 18 March 2014

Keywords:
Metal oxide
Carbon fibre
Pyrolysis
Lithium-ion battery
Conversion anode material

ABSTRACT

$CoFe_2O_4$ nanoparticles anchored into in-situ formed carbon nanofibres were synthesized by a simple solvent-free and template-free pyrolysis-oxidation process and have been investigated as a promising anode material for Li-ion batteries. Ferrocene and cobaltocene as precursor materials, act as both metal and carbon sources. Carbon contents in the composite can be easily adjusted by varying oxidation conditions. The as-prepared composites show a high and stable capacity. More than 700 mAh g^{-1} based on the total mass of the as-prepared composite was obtained in the composite with 36% carbon content after long-term cycling of 250 cycles. The superior electrochemical properties are suggested to be benefited from the synergistic effects by combining $CoFe_2O_4$ and carbon and also their intimate contact developed in the synthetic process. This work opens a facile and broadly applicable way for fabrication and utilization of metal oxide/mixed metal oxide-carbon composites for Li-ion batteries.

1. Introduction

Lithium-ion batteries (LIBs) as one of the important energy storage devices are quite attractive for not only popular portable devices but also upcoming electric vehicles. In order to meet the industry needs, the development of high performance rechargeable LIBs becomes increasingly important [1–5]. Many materials have been explored to replace graphite, which is popularly used as anode materials in the conventional LIBs and has a theoretical specific capacity of 372 mAh g^{-1} [6–9]. $CoFe_2O_4$ has been reported to act as an alternative anode material in LIBs owing to its high specific capacity of 914 mAh g^{-1} based on an eight-electron conversion

* Corresponding author. Tel.: +49 721 60828910; fax: +49 721 60826368.
E-mail addresses: shuhua.ren@kit.edu, s.ren@hotmail.de (S. Ren).

http://dx.doi.org/10.1016/j.jpowsour.2014.03.012
0378-7753/

reaction [10–25]. However, the large volume change and the poor electrical conductivity during the Li^+ insertion/extraction process limited its application, leading to capacity fade and poor cycling performance. To circumvent these problems, great efforts have been devoted on the combination of nanosized $CoFe_2O_4$ with versatile carbon materials of special forms, such as carbon nanotubes [10], graphene [11–12], or fibres [13–14], to improve the cycling behaviour and rate capability. Carbon can not only increase the electrical conductivity of the composite but also suppress the oxide particles aggregation during fabrication process, besides the buffering effect for large volume changes of the oxide during charging/discharging process [11]. Up to now, most strategies to fabricate such functional composite structure involve multi-step processes or the use of certain templates, surfactants, or special solvents, removal of which in the post treatment remain a major challenge and restrict their practical applications [10–25]. Thus, it is desirable to develop a facile straightforward synthetic strategy to generate such functional composite materials.

In this paper, a simple solvent-free and template-free process has been applied to the synthesis of a hybrid metal oxide system. $CoFe_2O_4$, as one of the representative binary metal oxides, was targeted due to its high specific Li-storage capacities. Pyrolysis of metallocene has been proven to be an effective way to produce fine carbon nanotube or nanofibre structures since the metal particles from the metallocene can catalyse the formation of nanotube or fibre structures [26–27]. Hence, $CoFe_2O_4$ encapsulated into an in-situ self-organized helical carbon nanofibre structure was fabricated by co-pyrolysis of mixed ferrocene and cobaltocene and subsequent oxidation of the pyrolysed product. No additional templates or solvents are involved in the fabrication process. Our group has previously testified Fe_3O_4/C system by using similar strategy and the synthesized material exhibited superior electrochemical behaviour [28]. Herein, further application of this method to a binary metal oxide system was performed and thereby the wide applicability of the strategy can be proven. Meanwhile, carbon contents in the composite can be easily adjusted through different oxidation conditions. The as-obtained nanocomposites can be directly used as active anode material without adding any extra conducting material for LIB application and exhibits a high and reversible capacity due to synergistic effects by combining metal oxide and carbon nanofibres.

2. Experimental

2.1. Material synthesis

In an argon-filled glove box, 0.663 g of Ferrocene (Alfa Aesar) and 0.337 g of Cobaltocene (Alfa Aesar) were manually mixed in an agate mortar for 30 min. The obtained dry mixture was sealed under argon atmosphere into a stainless steel reactor (inner diameter, 10.2 mm; length 46.7 mm) containing vacuum coupling radiation (VCR) type of fittings on both ends. The reactor was then directly placed into a preheated furnace at 700 °C. After 30 min, the reactor was taken out of the furnace and cooled down naturally. The remaining pressure inside the reactor was released carefully. A dry fine black powder was obtained and referred to as "$CoFe_2$/C". The as-obtained powder was transferred into a ceramic boat and then directly inserted into a preheated tube furnace at 400 °C for annealing 1, 5 or 10 min in air. After burning, the ceramic boat with oxidized powder inside was pulled out of the hot furnace and naturally cooled down to room temperature. The 1 min, 5 min or 10 min burned composites were referred to as "$CoFe_2O_4$/C-1 min", "$CoFe_2O_4$/C-5 min" and "$CoFe_2O_4$/C-10 min", respectively. Finally, the fine black powder of $CoFe_2O_4$/C composite was collected, and then transferred into the glovebox for further characterizations and LIB applications.

2.2. Characterization

Powder X-ray diffraction patterns (XRD) were collected using a PANalytical X'Pert diffractometer with Ni-filtered Cu Kα1,2 radiation (Kα1 = 1.5406 Å, Kα2 = 1.5444 Å) operated at 45 kV and 40 mA. The crystal structure parameters and crystallite sizes were refined by the Rietveld method [29] using the TOPAS software (Bruker AXS). Crystallite sizes are specified as the volume averaged column heights. The samples to be analysed were spread onto a silicon single crystal in the glovebox and sealed inside an airtight hood made of Kapton foil for XRD analysis. The morphology and microstructure of the nanocomposite were investigated using scanning electron microscopy (SEM; Leo-1530). The carbon contents of the $CoFe_2$/C and $CoFe_2O_4$/C-1 min, -5 min, -10 min nanocomposites were determined by elemental analysis (VarioMICRO cube from elementar- Analysensysteme GmbH).

The electrochemical measurements were conducted using two-electrode Swagelok-type cells with lithium metal working as both counter and reference electrodes. The working electrodes consist of 91 wt% $CoFe_2O_4$/C composite and 9 wt% of poly(vinyldifluoride-co-hexafluoropropylene) (SOLEF 21216/1001). Electrolyte employed in the test was 1 M $LiPF_6$ in ethylene carbonate (EC) and dimethyl carbonate (DMC) (1:1 v/v) (Merck). Glass fibre (GF/D; Whatman) was used as separator. Charge–discharge measurements were carried out galvanostatically over a potential range between 3.00 and 0.01 V (vs. Li/Li^+) using Arbin BT2000 multi-channel battery testing system. Cyclic voltammetry (CV, 0.01–3.00 V) was performed at various scan rates at room temperature using an electrochemical workstation (Zahner, Zennium).

3. Results and discussion

$CoFe_2O_4$ nanoparticles anchored into in-situ formed carbon nanofibres are produced by a facile two-step pyrolysis-oxidation route, as illustrated in Scheme 1. Through co-pyrolysis (step 1) of $Fe(C_5H_5)_2$ and $Co(C_5H_5)_2$ (2:1 in molar ratio) in a closed stainless steel reactor at 700 °C for 30 min, $CoFe_2$ alloy was formed, accompanied with in-situ formed carbon nanofibres and other gaseous products. The final oxide product of $CoFe_2O_4$ was obtained by subsequent oxidation (step 2) in air.

X-ray diffraction (XRD) pattern of the material after pyrolysis shows two diffraction peaks at 2θ of 44.77° and 65.28° (Fig. 1(a)), corresponding to the planes of (110) and (200) of the body centred cubic (bcc) phase $CoFe_2$, respectively [14,30,31]. A strong broad peak at 2θ of 26.58° from graphitic carbon was also observed. The formation of carbon nanofibres was observed by scanning electron microscopy (SEM) (data not shown). Upon subsequent oxidation of the $CoFe_2$/C composite in air at 400 °C, the $CoFe_2$ was oxidized into target spinel $CoFe_2O_4$ phase and carbon was partially burned away with little change in overall morphologies, as confirmed from the SEM images of the final products in Fig. 2. By varying the expose

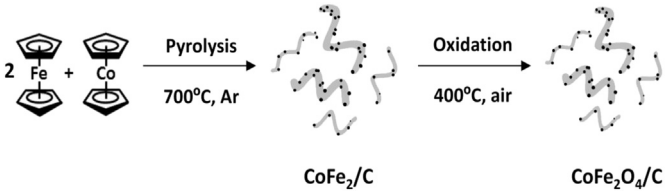

Scheme 1. Fabrication of $CoFe_2O_4$/C composite.

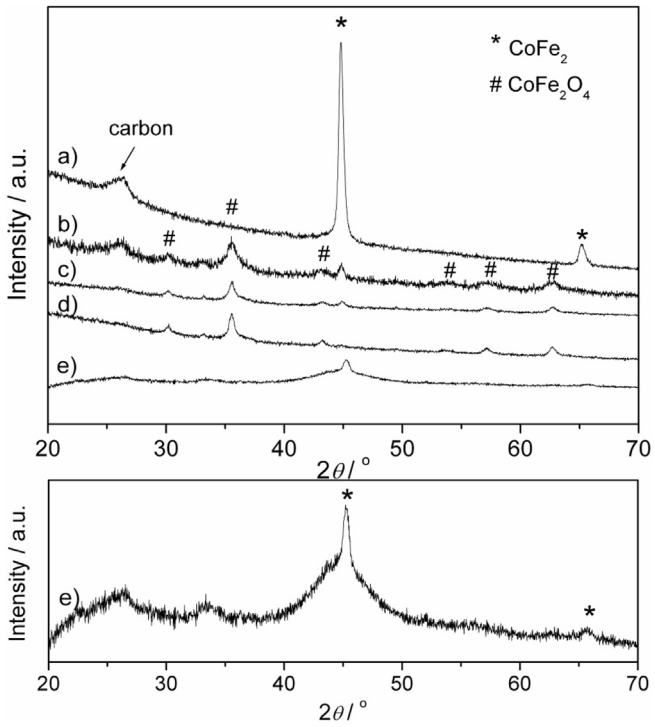

Fig. 1. XRD patterns of (a) pyrolysed $CoFe_2$/C nanocomposite, its target oxide products of (b) $CoFe_2O_4$/C-1 min, (c) $CoFe_2O_4$/C-5 min, (d) $CoFe_2O_4$/C-10 min through various air-oxidation time at 400 °C and (e) the lithiated $CoFe_2O_4$/C-1 min sample collected after 1st-discharged to 0.01 V at a current rate of 100 mA g^{-1}. Enlarged pattern for (e) (bottom).

time for oxidation reactions (1 min, 5 min, and 10 min), phase purity and carbon content in the composite can be adjusted. Thus, three composites were synthesized and denoted accordingly as "$CoFe_2O_4$/C-1 min", "$CoFe_2O_4$/C-5 min" and "$CoFe_2O_4$/C-10 min", respectively. N_2 isotherms of $CoFe_2$/C showed type IV curves (Figure S1), indicating a mesoporous structure. $CoFe_2$/C has a high Brunauer–Emmett–Teller (BET) surface area of 172 m^2 g^{-1}. After 5 min oxidation, $CoFe_2O_4$/C-5 min still gives a mesoporous structure with 113 m^2 g^{-1}. Relatively larger pore size and less pore volume were observed in 5 min oxidized sample. The XRD patterns confirm the formation of cubic spinel cobalt ferrite ($CoFe_2O_4$) with Fd3m space group (JCPDS No: 22-1086) (Fig. 1(b)–(d)). Note that $CoFe_2$ was not fully converted into $CoFe_2O_4$ with short oxidation reaction time of 1 min and 5 min. Residual $CoFe_2$ phase remains as observed from a small diffraction peak located at $2\theta = 44.8°$ in "$CoFe_2O_4$/C-1 min" and "$CoFe_2O_4$/C-5 min" (Fig. 1(b), (c)). Pure target $CoFe_2O_4$ phase was obtained for "$CoFe_2O_4$/C-10 min" (Fig. 1(d)) with relatively sharper diffraction peaks, indicating larger crystallite size. Crystallite sizes of the spinel ferrite phase, derived from the Rietveld refinement [29], are 10, 13 and 19 nm for the "$CoFe_2O_4$/C-1 min", "$CoFe_2O_4$/C-5 min" and "$CoFe_2O_4$/C-10 min", respectively. Despite the increasing of the crystallite size due to longer duration of oxidation, all the samples still remain nanocrystallites, indicating that in-situ formed carbon encapsulation inhibits effectively the growth of the ferrite crystal during the fabrication process. Varying the oxidation time, the carbon contents are reduced from 62% (pyrolysed composite of $CoFe_2$/C) to 45%, 36% and 25% for $CoFe_2O_4$/C-1 min, $CoFe_2O_4$/C-5 min, and $CoFe_2O_4$/C-10 min composites, respectively.

The morphologies of the $CoFe_2O_4$/C nanocomposites are shown in Fig. 2. The curly carbon nanofibres with different diameters in the range of 50–150 nm and various lengths are clearly observed in

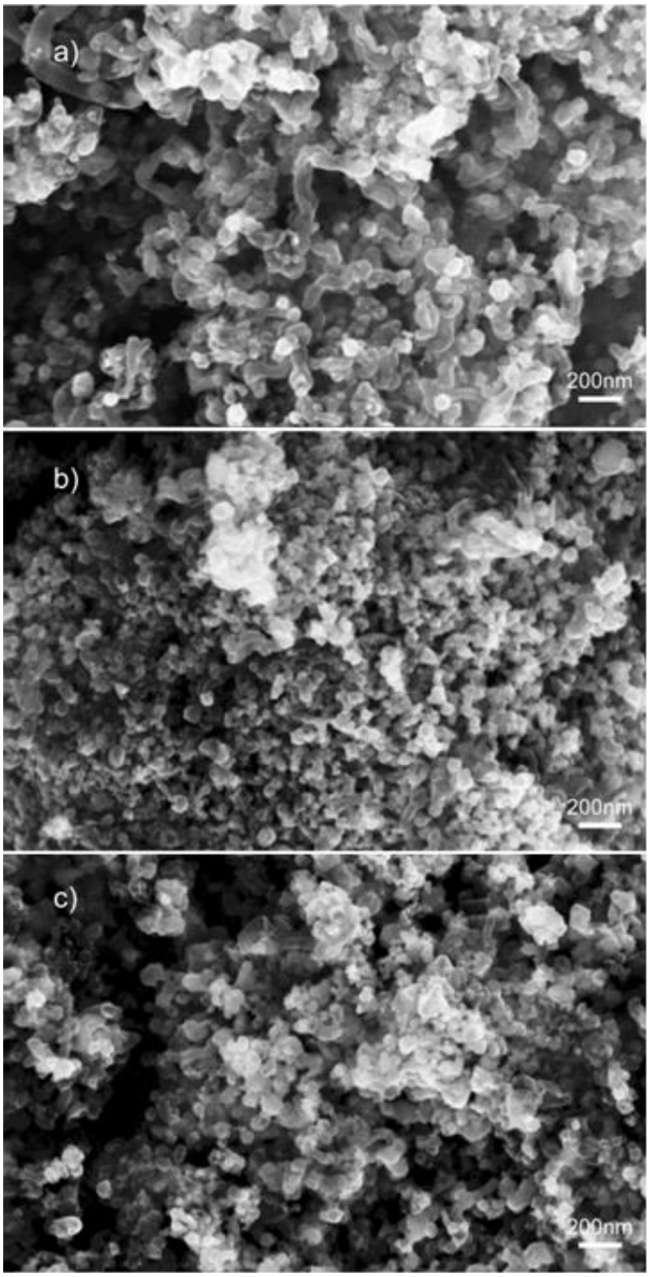

Fig. 2. SEM micrographs of the as-prepared (a) $CoFe_2O_4$/C-1 min, (b) $CoFe_2O_4$/C-5 min and (c) $CoFe_2O_4$/C-10 min.

$CoFe_2O_4$/C-1 min. Under controlled pyrolysis conditions, metal nanoclusters and reactive carbon are produced by decomposition of the corresponding metallocene, whereas carbon self-organized into a helical fibre structure. The metal nanoclusters are assumed to act as catalysts and nucleation centres for the formation and growth of curly and helical carbon nanofibres [28,32,33]. The loosely packed $CoFe_2O_4$ nanoparticles interconnected with carbon nanofibres could lead to special structure with a large amount of void space. Such structure is beneficial for the contact between active materials and electrolyte and releases the strain caused by volume expansion, and thus can improve cycling stability of the electrode [13–14]. However, the loosely packed structure is a disadvantage for the battery application due to the accordingly low volumetric energy density. In contrast to $CoFe_2O_4$/C-1 min, much less carbon nanofibres and denser structure were observed in both

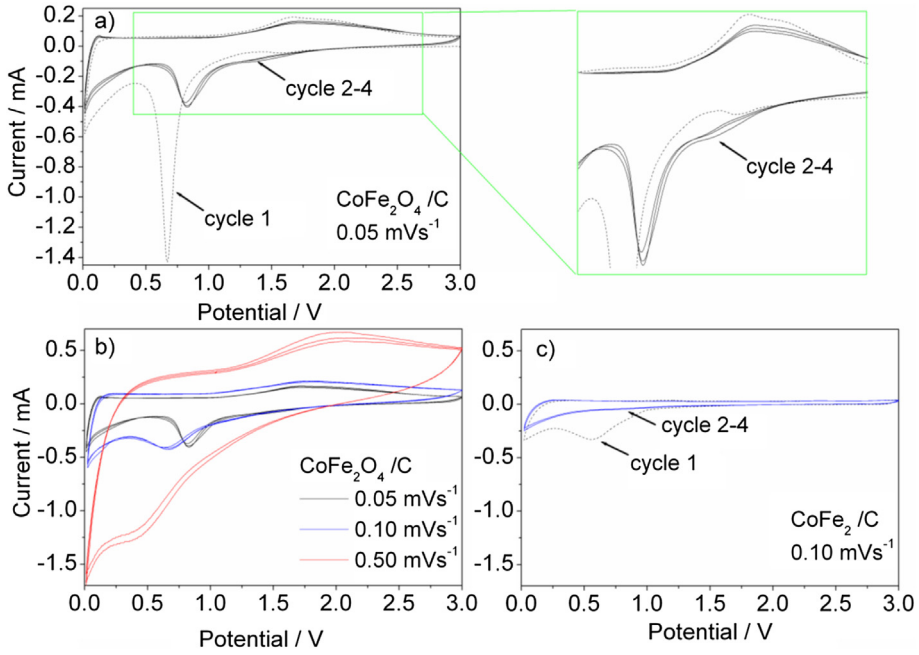

Fig. 3. CV curves of (a–b) the $CoFe_2O_4$/C-1 min composite and (c) $CoFe_2$/C composite at different scan rates between 0.01 and 3.00 V (vs. Li/Li^+) at room temperature.

$CoFe_2O_4$/C-5 min and $CoFe_2O_4$/C-10 min. Bigger and coarser particles were observed in $CoFe_2O_4$/C-10 min.

Ex situ XRD measurements of lithiated cobalt ferrite composite were also performed to examine the structure change after electrochemical lithiation. As-prepared $CoFe_2O_4$/C-1 min was discharged to 0.01 V at a current density of 100 mA g^{-1} and then collected for XRD analysis. As shown in Fig. 1(e), all the peaks corresponding to spinel cobalt ferrite vanished in the lithiated $CoFe_2O_4$/C-1 min composite. The small peak at $2\theta = 44.8^\circ$ corresponding to $CoFe_2$ alloy remains, which existed in the pristine material due to incomplete oxidation (Fig. 1(b)). Very broad peaks near Co–Fe metal phase were also observed (Fig. 1(e), enlarged pattern). The results indicate the existence of nanosized metallic phase after full conversion of $CoFe_2O_4$ upon discharging. Chu et al. reported that no diffraction peaks were observed for the lithiated electrode and concluded that the lithiated particles are smaller than the XRD coherence length [15]. The Li-driven conversion reaction leads to the complete reduction of the transition metal, whereas lithium ions link to oxygen to form Li_2O. It involves the complete disappearance of the structure of the starting oxide (spinel $CoFe_2O_4$). The conversion products are not randomly dispersed through the sample, but tightly bonded among themselves, almost preserving the morphology of the initial particle [16]. Without proper carbon confinement, large agglomerates of metal and Li_2O can be observed at the end of the cell discharge and the composite cannot sustain long battery cycling [16,34]. In our case, XRD result confirms the formation of metallic phase and the metallic phase remains nanosize after discharging thanks to the in-situ generated carbon encapsulation developed in the fabrication process.

The well-encapsulated $CoFe_2O_4$ nanoparticles by in-situ formed carbon nanofibres are developed through the fabrication process. The intimate binding between the metal oxide particles and carbon supports the final composite with superior electrochemical performance. To investigate the electrochemical behaviour, $CoFe_2O_4$/C composites against a lithium metal were assembled in Swagelok-type cells, without using additional conductive additives, and then subjected to cyclic voltammetry (CV) experiments (Fig. 3), followed by galvanostatic charge–discharge cycling (Fig. 4).

Fig. 3 shows the cyclic voltammograms (CV) of the $CoFe_2O_4$/C-1 min electrode at different scan rates. Both the cathodic and anodic peaks are positively shifted in the subsequent cycles due to structural modification after the first irreversible process

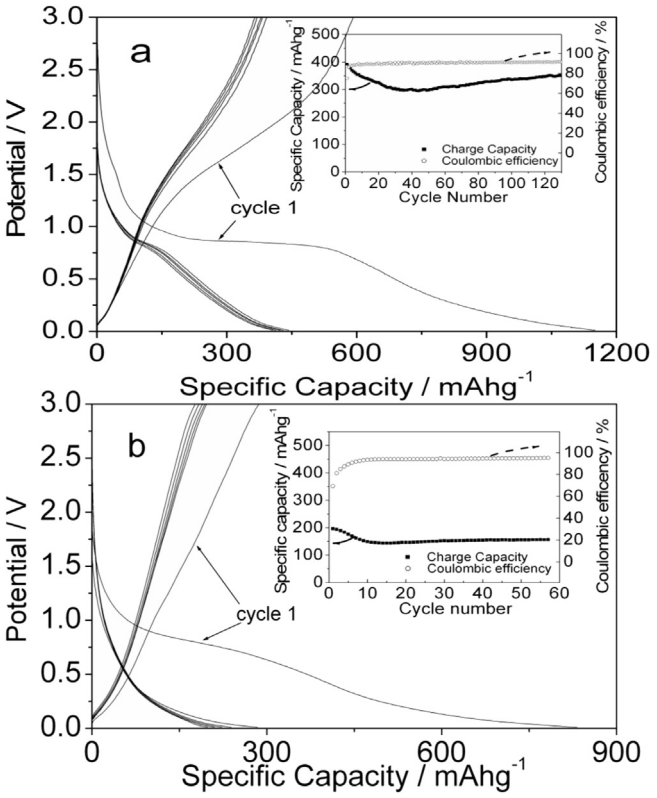

Fig. 4. Galvanostatic charge–discharge profiles (2nd – 6th cycles) of (a) $CoFe_2O_4$/C-1 min composite at 100 mA g^{-1} and (b) $CoFe_2$/C composite at 85 mA g^{-1} in the voltage range of 0.01–3.00 V after CV tests. The 1st cycle profiles in fresh battery cells are also shown. The insets show the corresponding plot of discharge capacity and coulombic efficiency as a function of cycle number.

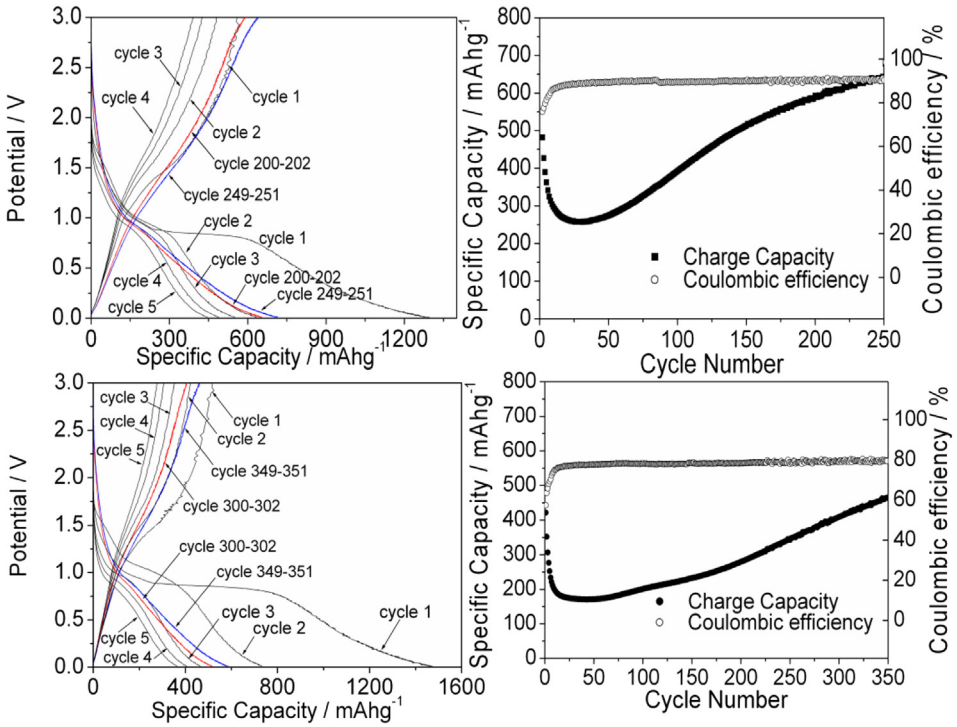

Fig. 5. Galvanostatic charge–discharge profiles and the corresponding plots of discharge capacity as a function of cycle number in $CoFe_2O_4$/C-5 min (up) and $CoFe_2O_4$/C-10 min (bottom) nanocomposites at 100 mA g^{-1} in the voltage range of 0.01–3.00 V.

[28,35–37]. From the second cycle onwards, the CV peak intensities and integral areas were almost unchanged, indicating good capacity retention of the cell upon cycling. Two cathodic peaks located at 0.81 and 1.40 V are related to the reduction of Fe^{3+} and Co^{2+} to their metallic states. The broad anodic peak can be ascribed to the oxidation reactions of the metallic Fe and Co. The results agree well with earlier studies [10–12]. The asymmetric nature of the CV curves suggests that the conversion reactions are only partially reversible and the complete structural recovery does not occur [10–12,37]. As the scan rate increases, the current increases rapidly and the conversion reactions can still be clearly observed.

In order to better understand the contribution of carbon to the overall performance of the $CoFe_2O_4$/C-1 min nanocomposite, further electrochemical investigations on $CoFe_2$/C were performed. CV curves for $CoFe_2$/C composite with the carbon amount equal to what exists in the $CoFe_2O_4$/C-1 min composite electrode are shown in Fig. 3(c). No apparent cathodic or anodic peak was observed in the $CoFe_2$/C electrode, except for the first cathodic scan, which indicates the occurrence of some irreversible reactions during the first cycle. By comparing the total stored charge–discharge capacities under the scan curves for both $CoFe_2O_4$/C-1 min (Fig. 3(b)) and $CoFe_2$/C (Fig. 3(c)) composites at 0.10 mV s^{-1}, it shows that the contribution of carbon is less than the overall capacities of $CoFe_2O_4$/C-1 min. Stable and reversible capacities of both $CoFe_2O_4$/C-1 min and $CoFe_2$/C composites are observed (Fig. 4), which is consistent with CV analysis. Based on the total mass of the composite, the overall discharge capacities of $CoFe_2O_4$/C-1 min and $CoFe_2$/C after extended CV analysis are 420 and 230 mAh g^{-1}, respectively. The good reversible capacity and cyclic stability may be attributed to the synergistic effects by combining metal oxide and carbon nanofibres, which provides good structural stability and good electrical conductivity. In addition, the flexible carbon fibres may accommodate volume changes of the composite during cycling.

Fig. 5 displays the galvanostatic charge and discharge profiles of $CoFe_2O_4$/C-5 min and $CoFe_2O_4$/C-10 min nanocomposites at a current rate of 100 mA g^{-1} and the corresponding cycling plots. In the first several cycles, charge–discharge capacities were decreasing dramatically over cycles for both $CoFe_2O_4$/C-5 min and $CoFe_2O_4$/C-10 min, indicating poor cycling stability in comparison to the performance in the composite $CoFe_2O_4$/C-1 min. This suggests that the in-situ formed carbon nanofibres in the composite may play a crucial role in cycling stability of the electrode material. Surprisingly, upon cycling, the capacity increased gradually for both $CoFe_2O_4$/C-5 min and $CoFe_2O_4$/C-10 min. After 200 and 250 cycles, $CoFe_2O_4$/C-5 min exhibited capacities of 656 mAh g^{-1} and 705 mAh g^{-1}, respectively. The theoretical capacities for the three composites were calculated to be 670, 719 and 779 mAh g^{-1}, respectively, on the basis of the corresponding mass ratios and theoretical capacities of $CoFe_2O_4$ (914 mAh g^{-1}) and carbon (372 mAh g^{-1}). Thus, the composite with less carbon content gives higher theoretical capacity for the final composite. It can be seen that the capacity of the $CoFe_2O_4$/C-5 min composite after 250 cycles almost reaches the theoretical capacity of this composite. For $CoFe_2O_4$/C-10 min, significant enhanced capacities of 360, 440, 515, 585 mAh g^{-1} were observed after 200, 250, 300, 350 cycles, respectively.

Such an activation process during battery cycling was also observed in the Fe_3O_4/C composite [28] and other $CoFe_2O_4$/C composites [13] reported previously. After extended cycling, the configuration of the oxide electrode rearranges, such that irreversible Li_2O formed during early cycles can be re-exposed and thus participate in the electrochemical reaction [38]. Wu et al. [13] attributed such behaviour to the result of an “electrochemical milling effect” [34]. The total surface area of the electrode materials and accordingly the contact area between the active material and electrolyte largely increases, which leads to increasing capacities with extended cycling. We believe such activation process with significant capacities rising after long-term cycling is also

supported by the special combination between $CoFe_2O_4$ and carbon in the composite. In contrast, in the bare $CoFe_2O_4$ sample [11], severe pulverization occurs during charge and discharge processes; the aggregation of $CoFe_2O_4$ nanoparticles can easily occur and cause very poor electrochemical cycling stability [10–12]. Consequently, the cycling capacities dropped constantly to less than 80 mAh g^{-1} after 50 cycles, as observed for the bare $CoFe_2O_4$ sample [11]. In $CoFe_2O_4$/C-5 min and $CoFe_2O_4$/C-10 min samples, although smaller fraction of carbon was left in the composite after longer oxidation time, intimate contact between oxide particles and carbon still remained, which supports the composite reviving under extended long cycling life. In the fabrication process of the $CoFe_2O_4$/C composites, the metal nanoclusters, formed upon decomposition of metallocene, catalyse the growth of carbon nanofibres. The strong connection between metal and carbon were thus created. The post annealing process during oxidation is assumed to be able to further strengthen such tight connection between the transformed metal oxide particles and carbon. Hence, the intimate interconnection between metal oxide and carbon are formed from the very beginning of the growth of metal oxide particles and carbon fibre formation. Such binding between oxide and carbon, preventing the oxide particles from aggregation during battery cycling, is suggested to be the major pillar of the composite and sustains the composite surviving from long-term cycling. The re-exposure of Li_2O formed during early cycles participates in the electrochemical process and finally provides activation process and leads to higher capacity after long cycling. Detailed microstructure analysis should be further performed in the future study to get a direct insight into the connection between $CoFe_2O_4$ and carbon.

Based on the previous results, $CoFe_2O_4$/C-1 min has the highest carbon content (45%) but also the most stable cycling stability in the electrochemical performance (Fig. 4(a)). $CoFe_2O_4$/C-10 min with the lowest carbon content (25%) showed relatively lowest capacities in the first 50 cycles (Fig. 5). However after long-term cycling, certain activation process with increasing capacities has been observed for all the three samples. $CoFe_2O_4$/C-5 min and $CoFe_2O_4$/C-10 min gave comparable and then much higher capacities than $CoFe_2O_4$/C-1 min after extended cycles. This indicates that an intimate contact between carbon and oxide material was formed upon such synthetic process and plays a crucial role in the activation process in the battery performance. The in-situ generated carbon encapsulation on the $CoFe_2O_4$ nanoparticles not only suppresses particle growth in the preparation process, but also inhibits particle aggregation during battery cycling, buffering the large volume expansion/contraction of $CoFe_2O_4$ during the conversion reactions.

4. Conclusion

A hybrid binary metal oxide/carbon material with $CoFe_2O_4$ nanoparticles anchored on self-grown carbon fibres was obtained through a simple two-step synthesis. No additional templates or solvents are involved in the synthetic process. By varying oxidation conditions, the carbon contents can be easily adjusted. Special intimate binding between mixed metal oxide nanoparticles and in-situ self-developed carbon fibres provided the final composite good cycling stability and inhibited the aggregation and pulverization of the oxide particles during battery cycling. Activation process with increased capacities after extended battery cycling was observed and assumed to be the result of re-exposure of the irreversible Li_2O formed during early cycles. A total capacity of 705 mAh g^{-1} was observed after 250 cycles, which is close to the theoretical capacity of the composite $CoFe_2O_4$/C-5 min. The presented fabrication route to get metal oxide/carbon nanocomposites is broadly applicable, providing new avenues for the engineering of electrode materials with enhanced performance.

Acknowledgements

Support by Karlsruhe Nano Micro Facility (KNMF) and Helmholtz Institute Ulm (HIU) is gratefully acknowledged.

Appendix A. Supplementary data

Supplementary data related to this article can be found at http://dx.doi.org/10.1016/j.jpowsour.2014.03.012.

References

[1] M.S. Whittingham, Chem. Rev. 104 (2004) 4271.
[2] A.S. Arico, P. Bruce, B. Scrosati, J.-M. Tarascon, W. van Schalkwijk, Nat. Mater. 4 (2005) 366.
[3] Y. Guo, J. Hu, L. Wan, Adv. Mater. 20 (2008) 2878.
[4] M. Fichtner, Phys. Chem. Chem. Phys. 13 (2011) 21186.
[5] M. Fichtner, J. Alloy Compd. 509 (2011) 529.
[6] P. Poizot, S. Laruelle, S. Grugeon, L. Dupont, J.-M. Taraschon, Nature 407 (2000) 496.
[7] J.-M. Tarascon, M. Armand, Nature 414 (2001) 359.
[8] J.B. Goodenough, Y. Kim, Chem. Mater. 22 (2010) 587.
[9] J. Cabana, L. Monconduit, D. Larcher, M.R. Palacin, Adv. Mater. 22 (2010) E170.
[10] Z. Zhang, Y. Wang, M. Zhang, Q. Tan, X. Lv, Z. Zhong, F. Su, J. Mater. Chem. A 1 (2013) 7444.
[11] S. Liu, J. Xie, C. Fang, G. Cao, T. Zhu, X. Zhao, J. Mater. Chem. 22 (2012) 19738.
[12] M. Zhang, M. Jia, Y. Jin, Q. Wen, C. Chen, J. Alloy Compd. 566 (2013) 131.
[13] L. Wu, Q. Xiao, Z. Li, G. Lei, P. Zhang, L. Wang, Solid State Ionics 215 (2012) 24.
[14] J. Xiang, X. Zhang, J. Li, Y. Chu, X. Shen, Chem. Phys. Lett. 576 (2013) 39.
[15] Y. Chu, Z. Fu, Q. Qin, Electrochim. Acta 49 (2004) 4915.
[16] P. Lavela, J.L. Tirado, M. Womes, J.C. Humas, J. Phys. Chem. C 113 (2009) 20081.
[17] Y. NuLi, Q. Qin, J. Power Sources 142 (2005) 292.
[18] M. Zhang, Y. Jin, Q. Wen, C. Chen, M. Jia, Appl. Surf. Sci. 277 (2013) 25.
[19] C. Vidal-Abarca, P. Lavela, J.L. Tirado, Solid State Ionics 181 (2010) 616.
[20] X. Yang, X. Wang, Z. Zhang, J. Cryst. Growth 277 (2005) 467.
[21] Z.H. Hua, R.S. Chen, C.L. Li, S.G. Yang, M. Lu, B.X. Gu, Y.W. Du, J. Alloy Compd. 427 (2007) 199.
[22] H. Xia, D. Zhu, Y. Fu, X. Wang, Electrochim. Acta 83 (2012) 166.
[23] Z.H. Li, T.P. Zhao, X.Y. Zhan, D.S. Gao, Q.Z. Xiao, G.T. Lei, Electrochim. Acta 55 (2010) 4594.
[24] Y. Sharma, N. Sharma, G.V. Subba Rao, B.V.R. Chowdari, Solid State Ionics 179 (2008) 587.
[25] P. Lavela, G.F. Ortiz, J.L. Tirado, E. Zhecheva, R. Stovanova, Sv Ivanova, J. Phys. Chem. C 111 (2007) 14238.
[26] R. Sen, A. Govindaraj, C.N.R. Rao, Chem. Phys. Lett. 267 (1997) 276.
[27] I. Martin-Gullon, J. Vera, J.A. Conesa, J.L. Gonzalez, C. Merino, Carbon 44 (2006) 1572.
[28] S. Ren, R. Prakash, D. Wang, V.S.K. Chakravadhanula, M. Fichtner, ChemSusChem 5 (2012) 1397.
[29] H.M. Rietveld, J. Appl. Cryst. 2 (1969) 65.
[30] L. Guo, X. Shen, F. Song, M. Liu, Y. Zhu, J. Sol Gel. Sci. Technol. 58 (2011) 524.
[31] M. Mohan, V. Chandra, S.S. Manoharan, J. Mater. Res. 23 (2008) 1849.
[32] S. Amelinckx, X.B. Zhang, D. Bernaerts, X.F. Zhang, V. Ivanov, J.B. Nagy, Science 265 (1994) 635.
[33] J.H. Xia, X. Jiang, C.L. Jian, C. Dong, Appl. Phys. Lett. 92 (2008) 063121.
[34] D. Larche, C. Masquelier, D. Bonnin, Y. Chabre, V. Masson, J.-B. Leriche, J.-M. Tarascon, J. Electrochem. Soc. 150 (2003) A133.
[35] J. Wang, C. Zhong, D. Wexler, N. Idris, Z. Wang, L. Chen, H. Liu, Chem. Eur. J. 17 (2011) 661.
[36] P. Lavela, J.L. Tirado, J. Power Sources 172 (2007) 379.
[37] Q. Zhang, Z. Shi, Y. Deng, J. Zheng, G. Liu, G. Chen, J. Power Sources 197 (2012) 305.
[38] M. Sathiya, A.S. Prakash, K. Ramesha, J.-M. Tarascon, A.K. Shukla, J. Am. Chem. Soc. 133 (2011) 16291.